Organic & Biomolecular Chemistry

www.rsc.org/obc

Volume 1 | Number 1 | Jan 2013 | Pages 1–100

ROYAL SOCIETY OF CHEMISTRY

ROYAL SOCIETY OF CHEMISTRY

www.rsc.org/obc

Journal Name

ARTICLE

Amphiphilic benzothiadiazole–triphenylamine–based aggregates that emit red light in water

Tsutomu Ishi-i,*[a] Ikumi Kitahara,[a] Shimpei Yamada,[b,c] Yusuke Sanada,[b,c] Kazuo Sakurai,[b,c] Asami Tanaka,[d] Naoya Hasebe,[d] Toshitada Yoshihara[d] and Seiji Tobita*[d]

In this study, we report a preparation and an aggregate emission behavior of an amphiphilic donor–acceptor dye, which is composed of a triphenylamine–benzothiadiazole donor–acceptor chromophore and two water-soluble hexa(ethylene glycol) chains. The dye is strongly fluorescent in nonpolar solutions such as cyclohexane and toluene, whereas the emission intensity is reduced in aprotic polar solutions such as DMF and acetonitrile. This fluorescence reduction correlates with the increase in polarity, by which the transition from a local excited state to a highly polarized excited state is facilitated, leading to increased nonradiative deactivation rate. Further, significant fluorescence quenching is observed in protic polar solutions such as ethanol and methanol. Hydrogen-bonding interactions between the dye and the protic solvent molecules further accelerate the deactivation rate. In contrast, in a water solution, red light emission is achieved distinctly at 622 nm with relatively large fluorescence quantum yield of 0.20. This red emission is related to the aggregation of the dye molecules grown up in water. The kinetic analysis from the fluorescence rate constant and nonradiative rate constant indicates that the nonradiative deactivation channel is restricted in water. The formed aggregate, which was indicated by transmittance electron microscopy as a spherical aggregate morphology with a diameter of 3–4 nm, provides a less polar hydrophobic space inside the aggregate structure, by which hydrogen-bonding and the subsequent quenching is restricted, leading to the reduction of the nonradiative deactivation rate.

Introduction

Recently, light-emitting organic dyes have been widely used as molecular probes or sensors in biological imaging techniques.[1,2] In biological applications, efficient light-emitting ability as well as sufficiently high solubility in biological aqueous media is required for molecular probes and sensors. However, most organic dyes are hydrophobic, and this facilitates aggregation in aqueous media. The intermolecular interactions in the aggregate state usually result in significant quenching of emission.[3] On the other hand, some types of organic dyes exhibit unusual emission enhancement, so-called aggregation-induced emission, in aqueous media.[4–17] The quenched state in aqueous media changes to an emissive state owing to the restriction of the intramolecular rotation arising from aggregate formation.[4,5] The aggregation-induced emission has a potential as turn-on type biological imaging reagents.[18] Such unusual emission enhancement was also found in the aggregation of some organic dyes bearing donor and acceptor moieties.[19–25] The donor–acceptor system has an advantage of longer-wavelength light emitting ability including red and infra-red light. This longer-wavelength emission is of particular importance in biological applications because the red and infra-red light falls within the biological optical window around 600-

1000 nm at which light maximally penetrates biological tissues.[26,27]
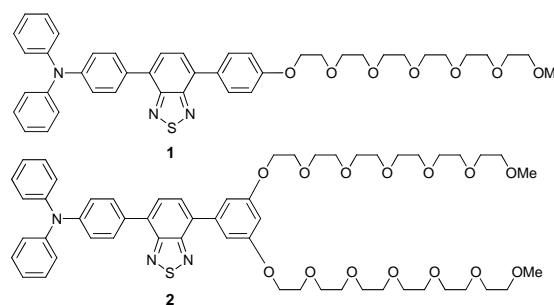
Scheme 1 Molecular structure of amphiphilic dyes **1** and **2**.

On the other hand, the emission in the donor–acceptor system is sensitive to the surrounding environment, such as the polarity and the hydrogen bonding ability of a solvent.[28,29] In a polar aqueous environment, the donor–acceptor dye tends to take a highly polarized excited state such as charge-transfer state,[22,23] from which the nonradiative deactivation channel is accelerated leading to a strong fluorescence quenching. In addition to restriction of the intramolecular rotation, the shielding of polar environment based on aggregation is

important to achieve efficient emission in the donor–acceptor system. Our aim in this study is to obtain further fundamental information in donor–acceptor emitting system as well as to achieve a red light emission in a water medium because the precedent systems have been studied in an organic solvent/water mixed medium such as THF/water.[19–25] Our concept is consisting of four factors. First, the donor–acceptor conjugation shifts the fluorescence band to produce longer-wavelength red light emission. Second, nonradiative deactivation arising from the polar environment is restricted by the aggregation, because the formed aggregate provides a less polar hydrophobic space inside the aggregate structure, leading to increased fluorescence radiative activation. Third, the use of triphenylamine as a donor moiety prevents the quenching problem arising from an ordered aggregation[3], because the nonplanar structure of triphenylamine disrupts packing and produces a less ordered structure.[30] Fourth, a versatile water-soluble functional group is introduced to create an amphiphilic donor–acceptor dye for achieving water solubility as well as preserving aggregate formation ability. Based on our precedent finding of donor–acceptor dye,[24] an amphiphilic triphenylamine–benzothiadiazole dye is designed by introducing hexa(ethylene glycol) chains as water-soluble functional groups (Scheme 1).[12,31] The fluorescence quantum yield and fluorescence lifetime were measured in various solvents to reveal the quenching mechanism in polar media as well as the emission enhancement in a water medium. The kinetic analysis from the fluorescence rate constant and nonradiative rate constant indicates a finding that the nonradiative deactivation channel arising from hydrogen-bonding is restricted by the aggregation, resulting in red light emission. In this study, we reports that the triphenylamine-benzothiadiazole dye bearing two hexa(ethylene glycol) chains provides red light emission behavior in the aggregate state.

Results and discussion

Donor–acceptor dyes **1** and **2** bearing hexa(ethylene glycol) chains were prepared from dibromobenzothiadiazole **3**[32,33] as shown in Scheme 2. The synthetic intermediates **4** and **6** bearing hydroxyl groups were used as references lacking hexa(ethylene glycol) chains. The structures were confirmed through the use of spectroscopic methods and elemental analysis. The reference dyes **4** and **6** can moderately dissolve in protic polar organic solvents such as ethanol and methanol. The solubility of **1** in polar solvents was sufficiently high because of the hexa(ethylene glycol) chain. However, dye **1** was poorly soluble in water. The water solubility of **1** could be significantly improved in **2** by introducing two hexa(ethylene glycol) chains. Thus, we studied the light emitting behavior mainly on **2** in various solvents including water.

The UV/vis absorption spectra of **1**, **2**, **4**, and **6** show an absorption band at around 440 nm, which can be attributed to the intramolecular charge-transfer transition arising from the donor–acceptor triphenylamine–benzothiadiazole chromophore.[26] The absorption band shifted very slightly depending on the solvent polarity (cyclohexane, toluene, THF, dichloromethane (DCM), DMF, acetonitrile, ethanol, methanol, water, etc.) (Fig. 1a and Figs. S1–S4†).

A strong dependence on solvent polarity was observed in the fluorescence spectra of dyes **1**, **2**, **4**, and **6**. The emission band shifted bathochromically, and the fluorescence quantum yield (Φ_f) decreased as the solvent polarity was increased (Fig. 1b and 1c, and Table 1; also see Figs. S5–S12†). When **2** was

dissolved in nonpolar cyclohexane and toluene, green-to-yellow light was emitted at 544–575 nm with a large Φ_f value of 0.85–0.88 (Table 1). The emission band shifted to the longer-wavelength red light region at 615 nm in THF, at 635 nm in DCM, at 660 nm in acetonitrile, and at 661 nm in DMF. Along with the bathochromic shift, the Φ_f value decreased from 0.88 in toluene to 0.77 in THF, 0.53 in DCM, 0.19 in DMF, and 0.15 in acetonitrile (Table 1). This fluorescence reduction can be explained based on the energy-gap law, in which the nonradiative deactivation rate increases exponentially upon decreasing the emission energy.[34] Moreover, this fluorescence reduction correlates with the increase in polarity, by which the transition from a local excited state to a highly polarized excited state such as an intramolecular charge transfer state is facilitated.[22,23] The polarized excited state is stabilized by solvation owing to the polar solvent molecules, leading to increased nonradiative deactivation rate.[24,25]
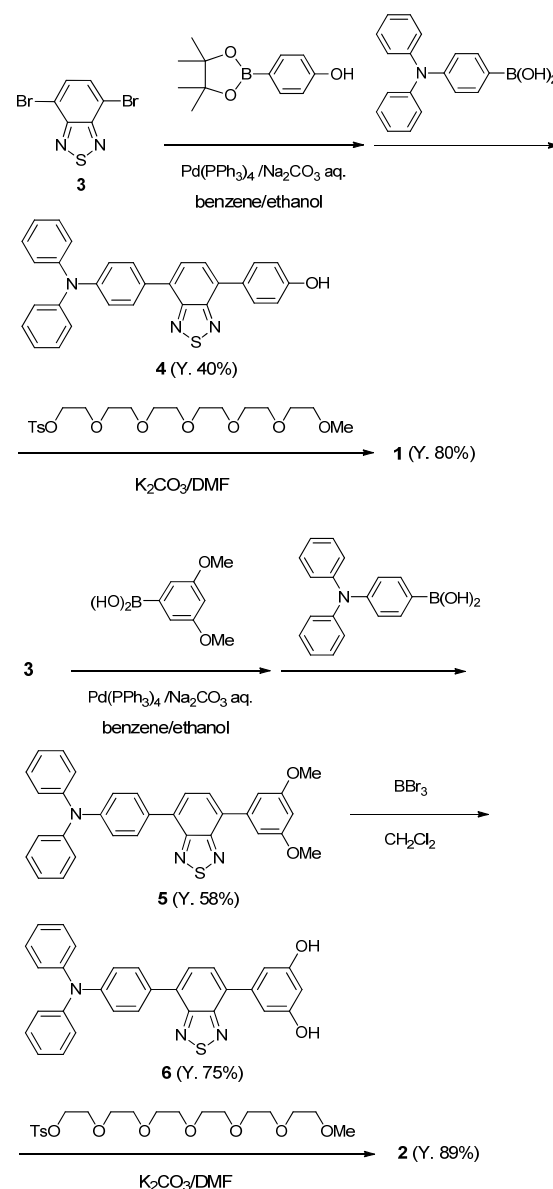
Scheme 2 Preparation of amphiphilic dyes **1** and **2**.

Significant fluorescence quenching was observed for **2** in protic polar media: the Φ_f value decreased to 0.014 in ethanol. Similarly, the values decreased remarkably to 0.005 in methanol and 0.002 in 2,2,2-trifluoroethanol, although these Φ_f values are less reliable compared with those in the other solvents owing to the limited sensitivity of our instrument (Table 1). In protic polar media, hydrogen-bonding interactions between the dye and the solvent molecules would induce significant fluorescence quenching.[35–37] This is supported by the fact that the degree of quenching coincided with the magnitude of the hydrogen-bond donor acidity (α) of solvent (ethanol (0.83) < methanol (0.93) < 2,2,2-trifluoroethanol (1.51)) (Table 1).[38] The positively charged hydrogen atom in the protic solvent likely interacts with the negatively charged nitrogen atom in the thiadiazole ring.[35] Deuterium isotope effects observed for Φ_f in ethanol support the quenching mechanism due to hydrogen-bonding interactions: the Φ_f value increased from 0.014 in ethanol to 0.025 in ethanol-d_1.[35] Thus, hydrogen-bonding interactions further accelerate the deactivation rate of **2** in the excited singlet state. Similar emission behavior, that is fluorescence reduction in polar aprotic solvents and significant fluorescence quenching in polar protic solvent, was observed for **1** bearing one hexa(ethylene glycol) chain (Table 1; also see Figs. S5 and S9†).

Fig. 1 (a) UV/Vis spectra (1.0×10^{-5} M) and (b) fluorescence spectra (1.0×10^{-6} M, excited at 440 nm) of **2** in cyclohexane, toluene, THF, DCM, DMF, methanol, and water. (c) Fluorescence images of **2** in cyclohexane, toluene, THF, DCM, DMF, methanol, and water (from left to right) at 1.0×10^{-5} M under UV light irradiation.

In a pure water solution of **2**, red light emission at 622 nm was observed with relatively large Φ_f (0.20) despite the fact that the solvent polarity as well as the hydrogen-bond donor acidity of water are higher than those of ethanol and methanol (Fig. 1b and 1c, and Table 1). The unusual emission is related to the aggregation of the donor–acceptor dyes grown up in water. The formed aggregate provides a less polar hydrophobic space inside the aggregate structure, by which solvation and hydrogen-bonding are restricted, leading to the reduction of the nonradiative deactivation rate (Fig. 2).[24] The unusual emission based on aggregation can be achieved even in a phosphate buffer solution (pH at 7.4) (Figs. S6 and S10†). The observed red light emission at 621 nm with Φ_f of 0.21 is useful for developing biological applications (Table 1). The emission behavior achieved in the aggregate state is explained persuasively by efficient emission in the bulk state, in which red fluorescence was emitted at 628 nm with Φ_f of 0.67 (Table 1 and Fig. S13†). The emission bands (621–628 nm) in the bulk state as well as in the aqueous media lie around those (615–635 nm) in the THF and DCM solutions. These results indicate that the polarity within the aggregate structure is similar to that of the less polar solvents.
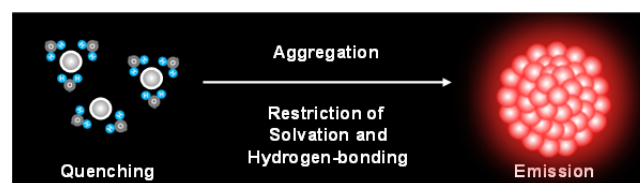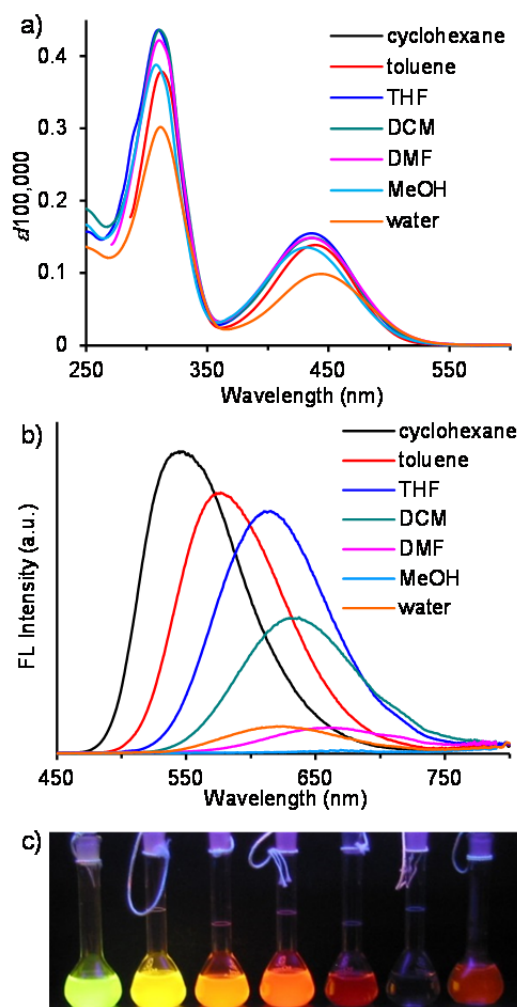

Fig. 2 Schematic for achieving red light emission based on the restriction of solvation and hydrogen-bonding upon aggregate formation.

The fluorescence lifetime of **2** was measured in various solvents to reveal the quenching mechanism in polar media as well as the emission enhancement in pure water medium.[12b,39] The fluorescence decay curves at the maximum emission wavelength could be fitted to a single- or double-exponential function (Fig. 3). The obtained τ_f values are listed in Table 1. The fluorescence rate constant (k_f) and nonradiative rate constant (k_{nr}) were calculated by using the following relations: $k_f = \Phi_f/\tau_f$ and $k_{nr} = (1-\Phi_f)/\tau_f$. For double-exponential decays, the intensity-averaged decay lifetime ($<\tau_f>$) was also calculated according to the equation $<\tau_f> = \Sigma(A_n\tau_{fn}^2)/\Sigma(A_n\tau_{fn})$,[40] where A_n is the amplitude of each exponential component. For double-exponential decays, the polar solvent solutions indicate a main component with large composition (>96%) along with a minor component. The minor component is likely attributed to trace amounts of aggregate species, which are formed through hydrophobic interactions in polar media. Thus, the rate constants were calculated by using the data of the main monomer component. In contrast, the two components in the water solution have comparable compositions of 58% and 42%. Theoretically, decay in the aggregated water solution is more complicated and is fitted to a multiple exponential because the

aggregates have size and length distributions. In this water solution, the averaged decay $<\tau_f>$ value was used to calculate the rate constants.

Table 1 Maximum absorption (λ_{abs}) and emission (λ_{em}) wavelengths, fluorescence quantum yield (Φ_f) and lifetime (τ_f), average fluorescence lifetime ($<\tau_f>$), radiative (k_f) and nonradiative (k_{nr}) rate constants of **2** (1.0×10^{-5} M) at 293 K, and solvent parameters (ε and α).

solvent	ε^a	α^b	λ_{abs} (nm)	λ_{em} (nm)	Φ_f	τ_f (ns) (fi [%])^c	$<\tau_f>$ (ns)^d	k_f (10^7 s^{-1})^e	k_{nr} (10^7 s^{-1})^e
cyclohexane	2.02	0.00	437	544	0.85	6.38	-	13	2.4
toluene	2.38	0.00	439	575	0.88	6.93	-	13	1.7
THF	7.52	0.00	436	615	0.77	8.03	-	9.6	2.9
DCM	8.93	0.30	437	635	0.53	7.20	-	7.4	6.5
DMF	38.3	0.00	435	661	0.19	3.06 (97) / 7.22 (3)	3.80	6.2^f	27^f
acetonitrile	37.5	0.19	427	660	0.15	2.62 (96) / 5.88 (4)	3.50	5.7^f	32^f
DMSO	46.7	0.00	437	669	0.14	-	-	-	-
ethanol	24.6	0.83	436	642	0.014	0.27 (97) / 4.37 (3)	0.37	5.3^f	370^f
ethanol-d_1	-	-	436	642	0.025	0.50 (96) / 5.79 (4)	0.71	5.0^f	200^f
2,2,2-trifluoroethanol	26.5	1.51	437	648	0.002^g	-	-	-	-
methanol	32.7	0.93	433	647	0.005^g	0.10 (96) / 4.10 (4)	0.25^g	-	-
water	80.4	1.17	444	622	0.20	2.40 (58) / 7.00 (42)	6.20	3.2^g	13^g
phosphate buffer (pH 7.4)	-	-	444	621	0.21	-	-	-	-
bulk	-	-	-	628	0.67	9.12	-	7.4	3.6

^{a} Dielectric constant of solvent. ^{b} Hydrogen-bond donor acidity of solvent.[36] ^{c} The value in parentheses is the fractional contribution of component i to the total steady-state intensity, which was calculated by $f_i = (A_i\tau_{fi}/\Sigma A_i\tau_{fi}) \times 100$. ^{d} The intensity-averaged decay lifetime ($<\tau_f>$) was calculated as follows: $<\tau_f> = \Sigma(A_n\tau_{fn}^2)/\Sigma(A_n\tau_{fn})$, in which A_n is the amplitude of each exponential term.[38] ^{e} The fluorescence rate constant (k_f) and nonradiative rate constant (k_{nr}) were calculated as follows: $k_f = \Phi_f/\tau_f$ and $k_{nr} = (1-\Phi_f)/\tau_f$. ^{f} The lifetime of the main component was used to calculate the rate constants. ^{g} The intensity-averaged decay lifetime ($<\tau_f>$) was used to calculate the rate constants. ^{g} The values are less reliable in view of the sensitivity of instruments.

Table 1 shows that in aprotic solvents, the Φ_f and τ_f values tend to reduce with an increase in the solvent polarity, whereas in protic solvents, the Φ_f and τ_f values show more pronounced decreases. With an increase in the polarity and hydrogen-bond donor ability of the solvent, the k_{nr} values are found to increase remarkably, although the k_f values decrease moderately. In the weakly emitting acetonitrile solution, dye **2** showed a shorter $<\tau_f>$ value of 3.50 ns with k_f value of 5.7×10^7 s^{-1} and k_{nr} value of 3.2×10^8 s^{-1}, compared to that (6.93 ns) in the strongly emitting toluene solution with k_f value of 1.3×10^8 s^{-1} and k_{nr} value of 1.7×10^7 s^{-1}. Furthermore, the $<\tau_f>$ value was reduced significantly to 0.37 ns in the quenching ethanol solution,

together with small k_f value of 5.3×10^7 s^{-1} and large k_{nr} value of 3.7×10^9 s^{-1}. In the methanol solution, dye **2** showed a much shorter lifetime ($<\tau_f> = 0.25$ ns), although the deconvoluted lifetime is less reliable in terms of the time resolution of our instrument. Compared to the toluene solution, the k_f value in ethanol was reduced by one order of magnitude, whereas the k_{nr} value was enhanced by two orders of magnitude. The significant enhancement of the k_{nr} value is ascribed to the acceleration of the nonradiative deactivation channel arising from hydrogen-bonding interactions between the excited dye molecules and protic solvent molecules. On the other hand, in the emitting water solution, the $<\tau_f>$ value increased to 6.20 ns together with the significant decrease in the k_{nr} value of 1.3×10^8 s^{-1}. The k_{nr} value in water was reduced by a factor of 28 times compared with that in ethanol. A similar trend with a significant decrease in k_{nr} value was also observed in the aggregated bulk state (Table 1). One can conclude that the restriction of solvation and hydrogen-bonding resulting from aggregation mainly leads to the reduction of the nonradiative deactivation rate.

To evaluate the unusual emission based on aggregation in more detail, the absorption and fluorescence spectra in **1**, **2**, **4** and **6** were measured in a methanol/water medium, in which the concentration of the dye was kept constant at 1.0×10^{-5} M and only the water fraction was increased from 0% to 100%. In **2**, both the absorption and the fluorescence spectra show a dependence on the percent water composition (Fig. 4). As the solution was increased to 50% water fraction, the significant fluorescence quenching remained unchanged. However, once the composition of the solution exceeded 60% water, the emission intensity increased and intensified progressively, with a final Φ_f value of 0.20, a 40-fold increase, at 100% (Figs. 5c and 6b). In low water volume, **2** exists in the monomeric form, and solvation and hydrogen-bonding are favored to cause quenching. In contrast, the amphiphilic dye molecules start to aggregate in high water volume, leading to the above-described unusual emission.
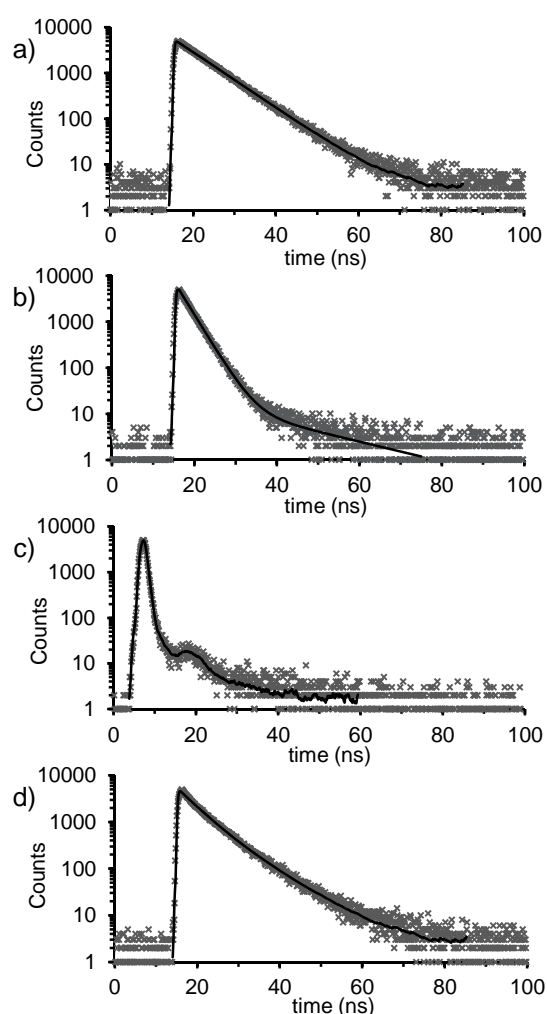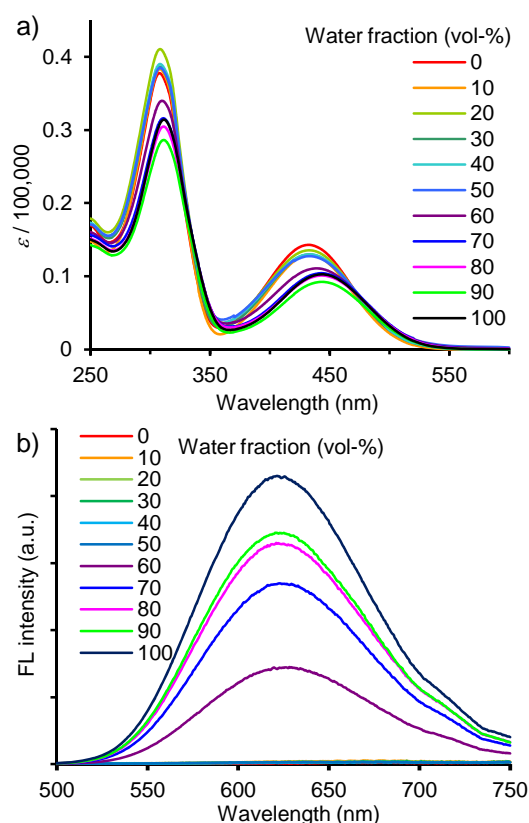

Fig. 3 Fluorescence decay curves of **2** at fluorescence maxima with excitation at 405 nm in (a) toluene, (b) acetonitrile, (c) ethanol, and (d) water at 1.0×10^{-5} M. Experimental decay curves were fitted with a single- or double-exponential function.

Fig. 4 (a) UV/Vis spectra and (b) fluorescence spectra (excited at 440 nm) of **2** in methanol/water (0−100% water fraction) at 1.0×10^{-5} M.

The aggregate formation in the emission region is supported by the shift of the absorption and emission bands. The absorption band shifted bathochromically from 433 nm (0% water fraction) to 444 nm (100%) (Fig. 5a). The bathochromic shift of 11 nm is most likely due to the formation of π-stacked aggregates with a *J*-type stacking mode, which is predicted by the molecular exciton model.[41] In addition, a hypsochromic shift of the emission band was observed, with values moving from 647 nm (0% water fraction) to 622 nm (100%) despite an increase in polarity (Fig. 5b). The hypsochromic shift of 25 nm

is most likely due to the local hydrophobic environment inside the aggregate structure, as described above.

Similar unusual emission behavior is observed in **1** bearing one hexa(ethylene glycol) chain (Figs. S14 and S15†), although the measurement cannot be performed at 100% water fraction. The transition from the quenched state to the emissive state started at 50% water fraction along with the bathochromic shift of the absorption band and the hypsochromic shift of the emission band. Finally, at 90% water fraction, red light emission in **1** was observed at 620 nm with Φ_f value of 0.33 (Figs. 5c and 6a).
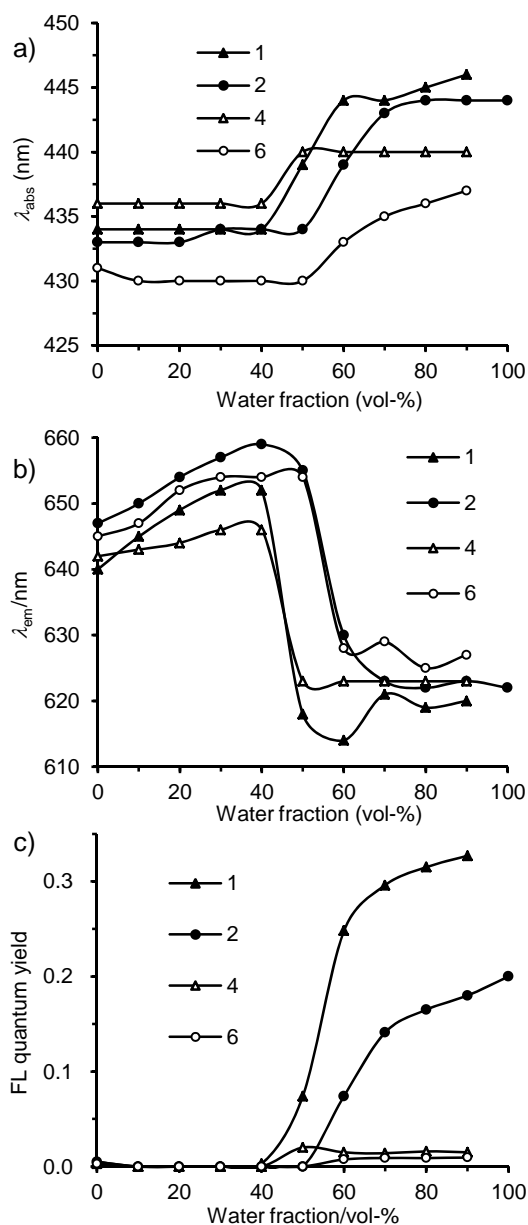

Fig. 5 Plots of the (a) absorption band, (b) fluorescence band, and (c) fluorescence quantum yield versus the water fraction of **1**, **2**, **4**, and **6** in methanol/water at 1.0×10^{-5} M.

On the other hand, the unusual emission was achieved very weakly in **4** and **6** lacking hexa(ethylene glycol) chains (Figs. 5c, 6c, and 6d; also see Figs. S16−19†), although the aggregate

was formed in high water volume as suggested by the absorption and fluorescence spectral change, transmittance electron microscopy, and dynamic light scattering (Fig. 5a and 5b; also see Figs. S20, S22, and S23). The Φ_f values were less than 0.01–0.02 even in the aggregate formation region (Fig. 5c). These results indicate that in **2** the hexa(ethylene glycol) chain plays an important role in red light emission in water, in addition to the contribution to the water solubility. In **4** and **6**, the very weak emission enhancement in methanol/water media is different from the previous finding that in THF/water media, the emission of the benzothiadiazole–triphenylamine dyes is efficiently enhanced upon aggregate formation.[24] This difference is likely attributed to the change in the surrounding environment from THF/water media to methanol/water ones. Actually, efficient emission enhancement was achieved in THF/water media: for **6** at 90% water fraction, red light emission was observed at 609 nm with Φ_f value of 0.30 together with a bathochromic shift of the absorption band and a hypsochromic shift of the emission band (Figs. S25−S28†).
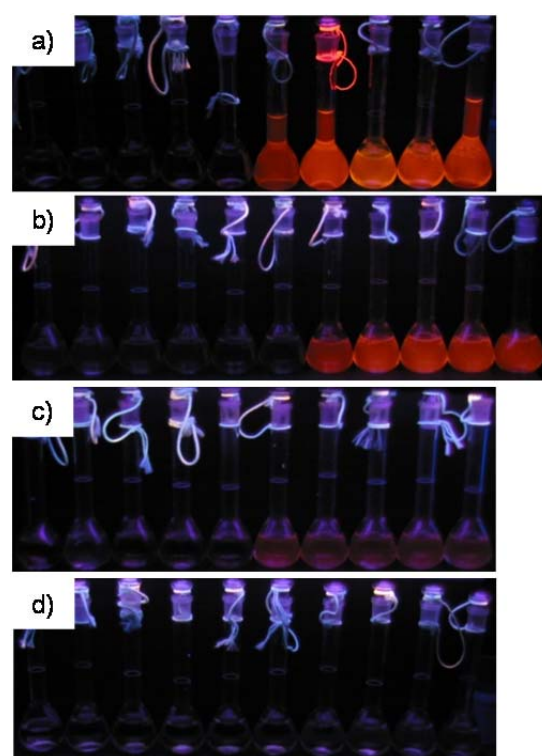

Fig. 6 Fluorescence images of (a) **1**, (b) **2**, (c) **4**, and d) **6** in methanol/water (10:0, 9:1, 8:2, 7:3, 6:4, 5:5, 4:6, 3:7, 2:8, 1:9, and 0:10 (v/v), from left to right) at 1.0×10^{-5} M under UV light irradiation. The images at 100% water fraction (0:10, v/v) were not shown in **1**, **4**, and **6**, because of the insolubility in water.

In **2**, a spherical aggregate morphology with a diameter of 3–4 nm is indicated by transmittance electron microscopy (TEM) observation (Fig. 7b), which takes a micellar-type stacking mode (Fig. S24†).[42] Micellar-type aggregate formation would be based on a subtle balance between the hydrophobic aromatic moiety and the hydrophilic hexa(ethylene glycol) moieties in the molecule. The hydrophilic hexa(ethylene glycol) chains, which are positioned at the surface of the micellar-type aggregate, likely disturb the polar solvent molecules approaching the aggregate core

composed of the hydrophobic triphenylamine–benzothiadiazole chromophores. Similar spherical aggregates were also formed in **1** with size of 50–100 nm (Fig. 7a). The spherical morphology likely results from the three-dimensional nonplanar structure of the triphenylamine moieties preventing ordered packing, as found in previous triphenylamine-based donor–acceptor dyes.[24,25] Compared to **2**, the large-sized aggregates in **1** can be detected by dynamic light scattering (Fig. S21†). Aggregate formation was confirmed at over 50% water fraction. The water fractions for which aggregate formation was detected coincide with the fractions for which the unusual emission was observed. These results indicate that the emission observed in water media is ascribed to aggregate formation.
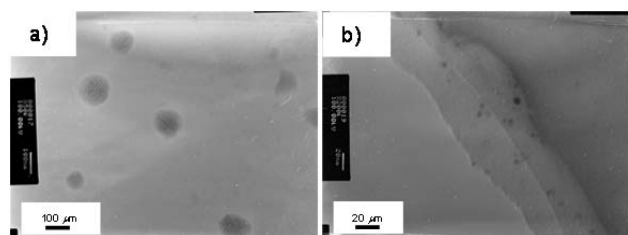

Fig. 7 TEM images of (a) **1** and (b) **2**. The samples were obtained by drop-casting from 1.0×10^{-4} M methanol/water (1:9 (v/v)) solution (**1**) and 1.0×10^{-4} M water solution (**2**) on carbon-coated copper grid.

Conclusions

In conclusion, we have demonstrated that red light emission is achieved in a water media based on the aggregation of a donor–acceptor dye bearing water-soluble functional groups. The proposed concept actually works, and it consists of four factors: (i) donor–acceptor conjugation to achieve red light emission; (ii) aggregation formation to restrict solvation, hydrogen-bonding, and the subsequent quenching; (iii) nonplanar structure of triphenylamine to avoid quenching arising from ordered packing; and (iv) introduction of water-soluble functional groups to create an amphiphilic dye. The nonradiative deactivation channel arising from solvation and hydrogen-bonding is restricted by an aggregation, leading to efficient red light emission. Furthermore, the restriction of intramolecular rotation contributes to the emission enhancement, as found in typical aggregation-induced emission dyes.[5]

The present red light emission can be achieved by two-photon excitation using a near-IR laser beam.[26] Two-photon excitation is very useful for developing a biological system because of the increased penetration depth in tissue with less photodamage and pin-point excitation by a focused laser beam.[43] We believe that the present results will provide useful information for achieving efficient light emission in the biological optical window based on a simple strategy for the aggregation of an amphiphilic donor–acceptor dye. The present findings on the change from the quenching state of monomer in water to the emissive state in aggregate will be developed to turn-on type probe and sensor.[18] We are currently in the process of creating biological imaging dye.

Experimental

General

All melting points are uncorrected. IR spectra were recorded on a JASCO FT/IR-470 plus Fourier transform infrared spectrometer, and measured as KBr pellets and on NaCl plate. ^{1}H and ^{13}C NMR spectra were determined in CDCl₃ with a JEOL JNM-AL 400 spectrometer. Residual solvent protons were used as internal standard and chemical shifts (δ) are given relative to tetramethylsilane (TMS). The coupling constants (J) are reported in hertz (Hz). Elemental analysis was performed at the Elemental Analytical Center, Kyushu University. Fast atom bombardment mass spectrometry (FAB-MS) spectra were recorded with a JEOL JMS-70 mass spectrometer with *m*-nitrobenzyl alcohol (NBA) as a matrix. Gel permeation chromatography (GPC) was performed with a Japan Analytical Industry LC-908 using JAIGEL-1H column (20 × 600 mm) and JAIGEL-2H column (20 × 600 mm) eluting with chloroform (3.0 mL/min). Analytical TLC was carried out on silica gel coated on aluminum foil (Merck 60 F₂₅₄). Column chromatography was carried out on silica gel (WAKO C300). THF was distilled from sodium and benzophenone under an argon atmosphere just before use. DCM was distilled from calcium hydride under an argon atmosphere just before use. DMF was distilled from calcium hydride under reduced pressure just before use. Tosylated derivative of hexa(ethylene glycol) monomethyl ether[12b,44] were prepared according to methods reported previously.

Instrumentation

The UV/Vis spectra were measured on a JASCO V-570 spectrophotometer in a 1.0 cm width cell. Fluorescence spectra were measured on a HITACHI F-4500 fluorescence spectrophotometer in a 1.0 cm width cell. The fluorescence quantum yield was measured with an absolute photoluminescence quantum yield measurement system (Hamamatsu, C9920-02), according to the method reported previously.[45] This instrument consisted of an integrating sphere equipped with a monochromatized Xe arc lamp as the light source and a multichannel spectrometer. The sensitivity of this system was fully calibrated for the spectral region 250-950 nm using deuterium and halogen standard light sources. A 10 mm path length quartz cuvette for solution samples was set in the integrating sphere. Dynamic light scattering (DLS) was measured on Photal OTSUKA ELECTRONICS ELSZ-1000 equipped with a 785 nm red laser source, using a fixed angle (90 °C). DLS experiments were performed at 25 °C in a 1.0 cm width quarts cell. A JEM-2100XS (JEOL) transmittance electron microscope was used for recording the transmittance electron microscopy (TEM) images. The accelerating voltage was 100 kV. TEM samples were prepared by placing a methanol/water solution (90% or 100% water fraction, 1.0×10^{-4} M) onto a carbon-coated copper grid (200 mesh), and then allowing the samples to dry for 5 h at room temperature and for additional 3 h under reduced pressure (0.1 torr). Fluorescence lifetime measurements were made by using a laser diode (405 nm, pulse width ~700 ps, repetition rate 10 kHz) as the excitation light source and a time-correlated single-photon counting fluorometer (Hamamatsu, Quantaurus-Tau C11367). The analysis of the fluorescence decay curves were carried out using the deconvolution method.

4-[4-(N,N-Diphenylamino)phenyl]-7-(4-hydroxyphenyl)-2,1,3-benzothiadiazole (4).

To a mixture of **3** (588 mg, 2.0 mmol) and tetrakis(triphenylphosphine)palladium (0) (231 mg, 0.2 mmol) in deaerated benzene (40 mL) were added 4-(4,4,5,5,-

tetramethyl-1,3,2-dioxaborolan-2-yl)phenol (528 mg, 2.4 mmol), deaerated ethanol (10 mL), and deaerated aqueous 2 M sodium carbonate solution (20 mL) at 60 ^{o}C under an argon atmosphere, and the resulting mixture was heated at 80 ^{o}C for 6 h. To the reaction mixture were added triphenylamine-4-boronic acid (694 mg, 2.4 mmol) and tetrakis(triphenylphosphine)palladium (0) (116 mg, 0.1 mmol) and the resulting mixture was heated at 80 ^{o}C for 16 h. The reaction mixture was poured into water and extracted with dichloromethane. The organic layer was washed with brine and water, dried over anhydrous magnesium sulfate, and evaporated in vacuo to dryness. The residue was purified by silica gel column chromatography (WAKO C300) eluting with dichloromethane to give **4** in 40% yield (375 mg, 0.795 mmol). An analytical sample obtained by recrystallization from hexane/dichloromethane. Orange prisms; mp 201–202 ^{o}C; ^{1}H NMR (400 MHz, CDCl$_3$): δ 5.01 (s, 1 H; OH), 7.00 (d, J = 8.3 Hz, 2 H; ArH), 7.07 (t, J = 8.3 Hz, 2 H; ArH), 7.18 (d, J = 8.3 Hz, 4 H; ArH), 7.23 (d, J =8.3 Hz, 2 H; ArH), 7.30 (t, J = 8.3 Hz, 4 H; ArH), 7.72 (d, J = 7.8 Hz, 1 H; ArH), 7.74 (d, J = 7.3 Hz, 1 H; ArH), 7.87 (d, J = 8.3 Hz, 2 H; ArH), 7.90 (d, J = 8.3 Hz, 2 H; ArH); ^{13}C NMR (100 MHz, CDCl$_3$) δ 115.55, 122.92, 123.29, 124.88, 127.38, 127.45, 129.34, 129.89, 130.19, 130.61, 130.98, 132.23, 132.27, 147.49, 148.00, 154.09, 154.24, 155.85; IR (KBr, cm^{-1}) 3435 (ν_{OH}), 3032, 1588, 1488, 1478, 1339, 1318, 1276, 1264, 1197, 1173, 893, 829, 750, 696, 618; MS (FAB): m/z 471 (M$^+$, 28%); HRMS (FAB): m/z calcd for C$_{30}$H$_{21}$N$_3$OS (M$^+$) 471.1405, found 471.1414. Anal. calcd for C$_{30}$H$_{21}$N$_3$OS (471.57): C, 76.41; H, 4.49; N, 8.91; Found: C, 76.49; H, 4.33; N, 8.94.

4-[4-(N,N-Diphenylamino)phenyl]-7-[4-(3,6,9,12,15,18-hexaoxanonadecyloxy)phenyl]-2,1,3-benzothiadiazole (1).
To a solution of 2-[2-(2-{2-[2-(2-methoxy-ethoxy)-ethoxy]-ethoxy}-ethoxy)-ethoxy]-ethyl p-tosylate (198 mg, 0.4 mmol) in dry DMF (4 mL) were added **4** (189 mg, 0.4 mmol) and crushed potassium carbonate (276 mg, 2.0 mmol) under an argon atmosphere and the resulting mixture was heated at 70 ^{o}C for 20 h. The reaction mixture was acidified by addition of aqueous hydrochloric acid (pH 2) at 0 ^{o}C and extracted with ethyl acetate. The organic layer was washed with brine (5 times), dried over anhydrous magnesium sulfate, and evaporated in vacuo to dryness. The residue was purified by silica gel column chromatography (WAKO C300) eluting with dichloromethane/ethyl acetate (4:1, v/v) to give **1** in 80% yield (240 mg, 0.32 mmol). Yellow orange viscous solid; ^{1}H NMR (400 MHz, CDCl$_3$) δ 3.37 (s, 3 H; OCH$_3$), 3.54 (t, J = 4.9 Hz, 2 H; CH$_2$), 3.62–3.72 (m, 16 H; CH$_2$), 3.76 (t, J = 4.9 Hz, 2 H; CH$_2$), 3.91 (t, J = 4.9 Hz, 2 H; CH$_2$), 4.23 (t, J = 4.9 Hz, 2 H; CH$_2$), 7.06 (t, J = 8.3 Hz, 4 H; ArH), 7.08 (d, J = 8.8 Hz, 2 H; ArH), 7.19 (d, J = 8.3 Hz, 4 H; ArH), 7.21 (d, J = 8.8 Hz, 2 H; ArH), 7.29 (t, J = 8.3 Hz, 4 H; ArH), 7.72 (d, J = 7.3 Hz, 1 H; ArH), 7.74 (d, J = 7.3 Hz, 1 H; ArH), 7.87 (d, J = 8.8 Hz, 2 H; ArH), 7.92 (d, J = 8.8 Hz, 2H; ArH); ^{13}C NMR (100 MHz, CDCl$_3$) δ 59.03, 67.56, 69.72, 70.50, 70.56, 70.60, 70.64, 70.88, 71.92, 114.79, 122.93, 123.28, 124.87, 127.41, 127.45, 129.34, 129.89, 130.16, 130.36, 131.02, 132.20, 132.27, 147.49, 147.97, 154.10, 154.25, 158.99; IR (NaCl, cm^{-1}) 3061, 3036, 2925, 2872, 1589, 1488, 1284, 1272, 1144, 1112, 823, 751, 695, 434, 408; MS (FAB): m/z 749 (M$^+$, 18%); HRMS (FAB): m/z calcd for C$_{43}$H$_{47}$N$_3$O$_7$S (M$^+$) 749.3135, found 749.3134. Anal. calcd for C$_{43}$H$_{47}$N$_3$O$_7$S (749.91): C, 68.87; H, 6.32; N, 5.60; Found: C, 68.50; H, 6.32; N, 5.52.

4-[4-(3,5-Dimethoxyphenyl)]-7-[4-(N,N-diphenylamino)phenyl]-2,1,3-benzothiadiazole (5).
To a mixture of **3** (1.17 g, 4.0 mmol) and tetrakis(triphenylphosphine)palladium (0) (462 mg, 0.4 mmol) in deaerated benzene (80 mL) were added 3,5-dimethoxyphenynoronic acid (874 mg, 4.8 mmol), deaerated ethanol (20 mL), and deaerated aqueous 2 M sodium carbonate solution (40 mL) at 60 ^{o}C under an argon atmosphere, and the resulting mixture was heated at 80 ^{o}C for 4 h. To the reaction mixture were added triphenylamine-4-boronic acid (1.39 g, 4.8 mmol) and tetrakis(triphenylphosphine)palladium (0) (116 mg, 0.1 mmol) and the resulting mixture was heated at 80 ^{o}C for 20 h. The reaction mixture was poured into water and extracted with dichloromethane. The organic layer was washed with brine and water, dried over anhydrous magnesium sulfate, and evaporated in vacuo to dryness. The residue was purified by silica gel column chromatography (WAKO C300) eluting with hexane/dichloromethane (1:1, v/v) to give **5** in 58% yield (1.19 g, 2.31 mmol). An analytical sample obtained by recrystallization from hexane/dichloromethane. Orange prisms; mp 155–156 ^{o}C; ^{1}H NMR (400 MHz, CDCl$_3$) δ 3.89 (s, 6 H; CH$_3$), 6.57 (t, J = 7.3 Hz, 1 H; ArH), 7.07 (t, J =8.1 Hz, 2 H; ArH), 7.12 (d, J = 7.3 Hz, 2 H; ArH), 7.19 (d, J =8.1 Hz, 2 H; ArH), 7.22 (d, J = 7.2 Hz, 2 H; ArH), 7.30 (t, J = 8.1 Hz, 4 H; ArH), 7.74 (d, J = 7.3 Hz, 1 H; ArH), 7.78 (d, J = 7.3 Hz, 1 H; ArH), 7.88 (d, J = 7.2, 2 H; ArH); ^{13}C NMR (100 MHz, CDCl$_3$) δ 55.16, 99.97, 107.21, 122.50, 123.02, 124.61, 126.82, 127.94, 129.04, 129.62, 130.48, 132.16, 132.75, 139.03, 147.12, 147.79, 153.70, 153.79, 160.51; IR (KBr, cm^{-1}) 3033, 2999, 2954, 2927, 2836, 1591, 1488, 1278, 1203, 1155, 1065, 826, 754, 695; MS (FAB): m/z 515 (M$^+$, 21%); HRMS (FAB): m/z calcd for C$_{32}$H$_{25}$N$_3$O$_2$S (M$^+$) 515.1667, found 515.1676. Anal. calcd for C$_{32}$H$_{25}$N$_3$O$_2$S (515.62): C, 74.54; H, 4.89; N, 8.15; Found: C, 74.61; H, 4.88; N, 8.10.

4-(3,5-Dihydroxyphenyl)-7-[4-(N,N-diphenylamino)phenyl]-2,1,3-benzothiadiazole (6).
To a solution of **5** (516 mg, 1.0 mmol) in dry dichloromethane (10 mL) were added dropwise 1 M boron tribromide dichloromethane solution (3.0 mL, 3.0 mmol) at 0 ^{o}C under an argon atmosphere and the resulting mixture was stirred at room temperature for 1 h. After the reaction mixture was cooled at 0 ^{o}C, the 1 M boron tribromide dichloromethane solution (3.0 mL, 3.0 mmol) was added dropwise and the resulting mixture was stirred at room temperature for 2 h. The reaction mixture was quenched by addition of water and dichloromethane at 0 ^{o}C. The obtained suspension including small amount of viscous solids was changed to homogeneous solution by addition of trace amount of acetone. The mixture was extracted with dichloromethane, washed with brine and water, dried over anhydrous magnesium sulfate, and evaporated in vacuo to dryness. The residue was purified by silica gel column chromatography (WAKO C300) eluting with dichloromethane/methanol (49:1, v/v) to give **6** in 75% yield (366 mg, 0.75 mmol). An analytical sample obtained by recrystallization from hexane/dichloromethane. Orange solid; mp 138–140 ^{o}C; ^{1}H NMR (400 MHz, CDCl$_3$) δ 5.03 (s, 2 H; OH), 6.46 (t, J = 1.5 Hz, 1 H; ArH), 7.05 (d, J = 1.5 Hz, 2 H; ArH), 7.07 (t, J = 7.8 Hz, 2 H; ArH), 7.19 (d, J = 7.8 Hz, 4 H; ArH), 7.22 (d, J = 8.8 Hz, 2 H; ArH), 7.30 (t, J = 7.8 Hz, 2H; ArH), 7.74 (d, J = 8.3 Hz, 1H; ArH), 7.75 (d, J = 8.3 Hz, 1 H; ArH), 7.87 (d, J = 8.8 Hz, 2 H; ArH); ^{13}C NMR (100 MHz, CDCl$_3$) δ 102.87, 109.02, 122.78, 123.38, 124.96, 127.11, 128.32, 129.36, 129.96, 130.68, 131.63, 133.28, 139.87, 147.45,

148.20, 153.95, 154.04, 156.87; IR (KBr, cm^{-1}) 3519 (ν_{OH}), 3272 (ν_{OH}), 3058, 3034, 1591, 1486, 1326, 1279, 1165, 1001, 827, 757, 695; MS (FAB): *m/z* 487 (M$^+$, 13%); HRMS (FAB): *m/z* calcd for C$_{30}$H$_{21}$N$_3$O$_2$S (M$^+$) 487.1354, found 487.1361. Anal. calcd for C$_{30}$H$_{21}$N$_3$O$_2$S (487.57): C, 73.90; H, 4.34; N, 8.62.; Found: C, 73.81; H, 4.34; N, 8.59.

4-[4-(N,N-Diphenylamino)phenyl]-7-[3,5-bis(3,6,9,12,15,18-hexaoxanonadecyloxy)phenyl]-2,1,3-benzothiadiazole (2).

To a solution of 2-[2-(2-{2-[2-(2-methoxy-ethoxy)-ethoxy]-ethoxy}-ethoxy)-ethyl *p*-tosylate (198 mg, 0.4 mmol) in dry DMF (4 mL) were added **6** (98 mg, 0.2 mmol) and crushed potassium carbonate (276 mg, 2.0 mmol) under an argon atmosphere and the resulting mixture was heated at 70 ^{o}C for 20 h. The reaction mixture was acidified by addition of aqueous hydrochloric acid (pH 2) at 0 ^{o}C and extracted with ethyl acetate. The organic layer was washed with brine (5 times), dried over anhydrous magnesium sulfate, and evaporated in vacuo to dryness. The residue was purified by silica gel column chromatography (WAKO C300) eluting with dichloromethane/methanol (49:1, v/v) and by GPC eluting with chloroform to give **2** in 89% yield (186 mg, 0.18 mmol). Orange viscous solid; ^{1}H NMR (400 MHz, CDCl$_3$) δ 3.37 (s, 6 H; OCH$_3$), 3.54 (t, *J* = 4.9 Hz, 4 H; CH$_2$), 3.63–3.71 (m, 32 H; CH$_2$), 3.76 (t, *J* = 4.9 Hz, 4 H; CH$_2$), 3.90 (t, *J* = 4.9 Hz, 4 H; CH$_2$), 4.21 (t, *J* = 4.9 Hz, 4 H; CH$_2$), 6.60 (t, *J* = 2.0 Hz, 1 H; ArH), 7.01 (t, *J* = 7.3 Hz, 2 H; ArH), 7.14 (t, *J* = 2.0 Hz, 2 H; ArH), 7.19 (d, *J* = 7.8 Hz, 4 H; ArH), 7.20 (d, *J* = 7.3 Hz, 2 H; ArH), 7.32 (t, *J* = 7.3 Hz, 4 H; ArH), 7.75 (d, *J* = 7.3 Hz, 1 H; ArH), 7.76 (d, *J* = 7.3 Hz, 1 H; ArH), 7.87 (d, *J* = 8.7 Hz, 2 H; ArH); ^{13}C NMR (100 MHz, CDCl$_3$) δ 59.00, 67.60, 69.70, 70.49, 70.55, 70.56, 70.62, 101.60, 108.38, 122.82, 123.32, 124.91, 127.15, 128.25, 129.34, 129.94, 130.82, 132.37, 133.03, 139.23, 147.45, 148.10, 154.02, 154.05, 159.92; IR (KBr, cm^{-1}) 3058, 3035, 2872, 1592, 1511, 1488, 1452, 1350, 1328, 1281, 1174, 1108, 830, 698; MS (FAB): *m/z* 1043 (M$^+$, 22%); HRMS (FAB): *m/z* calcd for C$_{56}$H$_{73}$N$_3$O$_{14}$S (M$^+$) 1043.4813, found 1043.4807.

Acknowledgements

Notes and references

^{a} Department of Biochemistry and Applied Chemistry, Kurume National College of Technology, 1-1-1 Komorino, Kurume 830-8555, Japan. E-mail: ishi-i@kurume-nct.ac.jp

^{b} Department of Chemistry and Biochemistry, The University of Kitakyushu, 1-1 Hibikino, Wakamatsu-ku, Kitakyushu 808-0135, Japan.

^{c} Structural Materials Science Laboratory SPring-8 Center, RIKEN, Harima Institute Research, 1-1-1 Kouto, Sayo, Sayo, Hyogo 679-5148, Japan.

^{d} Division of Molecular Science, Graduate School of Science and Technology, Gunma University, 1-5-1 Tenjin-cho, Kiryu, Gunma 376-8515, Japan.

† Electronic Supplementary Information (ESI) available: the UV/Vis and fluorescence spectra of **1**, **2**, **4** and **6** in various solvents, the fluorescence images of **1**, **2**, **4** and **6** in various solvents, the UV/Vis and fluorescence spectra of **1**, **4** and **6** in methanol/water, the TEM images of **4** and **6**, the DLS charts of **1**, **4** and **6** in methanol/water, the small-angle X-ray scattering profile of **2**, the UV/Vis and fluorescence spectra of **6** in THF/water, and the ^{1}H and ^{13}C spectra of **1**, **2**, **4**, **5** and **6**. See DOI: 10.1039/b000000x/

1. (a) K. E. Sapsford, L. Berti and I. L. Medintz, *Angew. Chem. Int. Ed.*, 2006, **45**, 4562–4588; (b) J. Liu, Z. Cao and Y. Lu, *Chem. Rev.*, 2009, **109**, 1948–1998; (c) H. Kobayashi, M. Ogawa, R. Alford, P. L. Choyke and Y. Urano, *Chem. Rev.*, 2010, **110**, 2620–2640; (d) Y. Takaoka, A. Ojida and I. Hamachi, *Angew. Chem. Int. Ed.*, 2013, **52**, 4088–4106; (e) R. W. Sinkeldam, N. J. Greco and Y. Tor, *Chem. Rev.*, 2010, **110**, 2579–2619; (f) J. Han and K. Burgess, *Chem. Rev.*, 2010, **110**, 2709–2728.

2. (a) G. Zlokarnik, P. A. Negulescu, T. E. Knapp, L. Mere, N. Burres, L. Feng, M. Whitney, K. Roemer and R. Y. Tsien, *Science*, 1998, **279**, 84–88; (b) B. A. Griffin, S. R. Adams and R. Y. Tsien, *Science*, 1998, **281**, 269–272; (c) A. Ojida, Y. Mito-oka, M. Inoue and I. Hamachi, *J. Am. Chem. Soc.*, 2006, **124**, 6256–6258; (d) H. Nonaka, S. Fujishima, S. Uchinomiya, A. Ojida and I. Hamachi, *J. Am. Chem. Soc.*, 2010, **132**, 9301–9309; (e) Y. Taniguchi, R. Kawaguchi and S. Sasaki, *J. Am. Chem. Soc.*, 2011, **133**, 7272–7275; (f) T. Tamura, Y. Kioi, T. Miki, S. Tsukiji and I. Hamachi, *J. Am. Chem. Soc.*, 2013, **135**, 6782–6785; (g) I. Takashima, M. Kinoshita, R. Kawagoe, S. Nakagawa, M. Sugimoto, I. Hamachi and A. Ojida, *Chem. Eur. J.*, 2014, **20**, 2184–2192; (h) S.-n. Uno, M. Kamiya, T.Yoshihara, K. Sugawara, K. Okabe, M. C. Tarhan, H. Fujita, T. Funatsu, Y. Okada, S. Tobita and Y. Urano, *Nature Chem.*, 2014, **6**, 681–689.

3. (a) H. Langhals, T. Potrawa, H. Noth and G. Linti, *Angew. Chem. Int. Ed. Engl.*, 1989, **28**, 478–480; (b) H. Langhals, O. Krotz, K. Polborn, P. Mayer, *Angew. Chem. Int. Ed.*, 2005, **44**, 2427–2428.

4. J. Luo, Z. Xie, J. W. Y. Lam, L. Cheng, H. Chen, C. Qiu, H. S. Kwok, X. Zhan, Y. Liu, D. Zhu and B. Z. Tang, *Chem. Commun.*, 2001, 1740–1741.

5. J. Mei, Y. Hong, J. W. Y. Lam, A. Qin, Y. Tang and B. Z. Tang, *Adv. Mater.*, 2014, **26**, 5429–5479.

6. (a) Y. Hong, J. W. Y. Lam and B. Z. Tang, *Chem. Commun.* 2009, 4332–4353; (b) M. Wang, G. Zhang, D. Zhang, D. Zhu and B. Z. Tang, *J. Mater. Chem.*, 2010, **20**, 1858–1867; (c) Y. Hong, J. W. Y. Lam and B. Z. Tang, *Chem. Soc. Rev.*, 2011, **40**, 5361–5388.

7. R. Deans, J. Kim, M. R. Machacek and T. M. Swager, *J. Am. Chem. Soc.*, 2000, **122**, 8565–8566.

8. B.-K. An, S.-K. Kown, S.-D. Jung and S. Y. Park, *J. Am. Chem. Soc.*, 2002, **124**, 14410–14415.

9. (a) Q. Zeng, Z. Li, Y. Dong, C. Di, A. Qin, Y. Hong, L. Ji, Z. Zhu, C. K. W. Jim, G. Yu, Q. Li, Z. Li, Y. Liu, J. Qin and B. Z. Tang, *Chem. Commun.*, 2007, 70–72; (b) Z. Li, Y. Q. Dong, J. W. Y. Lam, J. Sun, A. Qin, M. Häußler, Y. P. Dong, H. H. Y. Sung, I. D. Williams, H. S. Kwok and B. Z. Tang, *Adv. Funct. Mater.*, 2009, **19**, 905–917; (c) Z. Zhao, D. Liu, F. Mahtab, L. Xin, Z. Shen, Y. Yu, C. Y. K. Chan, P. Lu, J. W. Y. Lam, H. H. Y. Sung, I. D. Williams, B. Yang, Y. Ma and B. Z. Tang, *Chem. Eur. J.*, 2011, **17**, 5998–6008.

10   (a) Y. Dong, J. W. Y. Lam, A. Qin, Z. Li, J. Sun, H. H.-Y. Sung, I. D. Williams and B. Z. Tang, *Chem. Commun.*, 2007, 40–42; (b) R. Hu, J. L. Maldonado, M. Rodriguez, C. Deng, C. K. W. Jim, J. W. Y. Lam, M. M. F. Yuen, G. Ramos-Ortiz and B. Z. Tang, *J. Mater. Chem.*, 2012, **22**, 232–240; (c) J. Wang, J. Mei, R. Hu, J. Zhi Sun, A. Qin and B. Z. Tang, *J. Am. Chem. Soc.*, 2012, **134**, 9956–9966; (d) J. Tong, Y. Wang, J. Mei, J. Wang, A. Qin, J. Z. Sun and B. Z. Tang, *Chem. Eur. J.*, 2014, **20**, 4661–4670.

11   (a) B.-K. An, D.-S. Lee, J.-S. Lee, Y.-S. Park, H.-S. Song and S. Y. Park, *J. Am. Chem. Soc.*, 2004, **126**, 10232−10233; (b) S.-J. Lim, B.-K. An, S. D. Jung, M.-A. Chung and S. Y. Park, *Angew. Chem. Int. Ed.*, 2004, **43**, 6346–6350; (c) B.-K. An, S.-K. Kwon and S. Y. Park, *Angew. Chem. Int. Ed.*, 2007, **46**, 1978–1982; (d) S.-J. Yoon, J. W. Chung, J. Gierschner, K. S. Kim, M.-G. Choi, D. Kim and S. Y. Park, *J. Am. Chem. Soc.*, 2010, **132**, 13675–13683.

12   (a) T. Hirose and K. Matsuda, *Chem. Commun.*, 2009, 5832–5834; (b) T. Hirose, K. Higashiguchi and K. Matsuda, *Chem. Asian J.*, 2011, **6**, 1057–1063.

13   (a) S. Kamino, Y. Horio, S. Komeda, K. Minoura, H. Ichikawa, J. Horigome, A. Tatsumi, S. Kaji, T. Yamaguchi, Y. Usami, S. Hirota, S. Enomoto and Y. Fujita, *Chem. Commun.*, 2011, **46**, 9013–9015; (b) S. Kamino, A. Muranaka, M. Murakami, A. Tatsumi, N. Nagaoka, Y. Shirasaki, K. Watanabe, K. Yoshida, J. Horigome, S. Komeda, M. Uchiyama and S. Enomoto, *Phys. Chem. Chem. Phys.*, 2013, **15**, 2131–2144.

14   (a) Z. Ning, Z. Chen, Q. Zhang, Y. Yan, S. Qian, Y. Cao and H. Tian, *Adv. Funct. Mater.*, 2007, **17**, 3799–3807; (b) Y. Jiang, Y. Wang. J. Hua, J. Tang, B. Li, S. Qian and H. Tian, *Chem. Commun.*, 2010, **46**, 4689–4691; (c) B. Wang, Y. Wang, J. Hua, Y. Jiang, J. Huang, S. Qian and H. Tian, *Chem. Eur. J.*, 2011, **17**, 2647–2655.

15   (a) T. Sanji, K. Shiraishi and M Tanaka, *ACS Appl. Mater. Int.*, 2009, **1**, 270–273; (b) T. Sanji, K. Shiraishi, M. Nakamura and M. Tanaka, *Chem. Asian J.*, 2010, **5**, 817–824.

16   (a) S. Kim, Q. Zheng, G. S. He, D. J. Bharali, H. E. Pudavar, A. Baev and P. N. Prasad, *Adv. Funct. Mater.*, 2006, **16**, 2317–2323; (b) M. Shimizu, H. Tatsumi, K. Mochida, K. Shimono and T. Hiyama, *Chem. Asian J.*, 2009, **4**, 1289–1297; (c) B. Xu, J. He, Y. Dong, F. Chen, W. Yu and W. Tian, *Chem. Commun.*, 2011, **46**, 6602–6604; (d) X. Zhang, Z. Chi, H. Li, B. Xu, X. Li, W. Zhou, S. Liu, Y. Zhang and J. Xu, *Chem. Asian J.*, 2011, **6**, 808–811; (e) T. Noguchi, T. Shiraki, A. Dawn, Y. Tsuchiya, L. T. N. Lien, T. Yamamoto and S. Shinkai, *Chem. Commun.*, 2012, **48**, 8090–8092; (f) R. Yoshii, A. Nagai, K. Tanaka and Y. Chujo, *Chem. Eur. J.*, 2013, **19**, 4506–4512.

17   L. Yao, S. Zhang, R. Wang, W. Li, F. Shen, B. Yang and Y. Ma, *Angew. Chem. Int. Ed.*, 2014, **53**, 2119 –2123.

18   (a) Y. Hong, H. Xiong, J. W. Y. Lam, M. Häußler, J. Liu, Y. Yu, Y. Zhong, H. H. Y. Sung, I. D. Williams, K. S. Wong and B. Z. Tang, *Chem. Eur. J.*, 2010, **16**, 1232–1245; (b) Y. Liu, C. Deng, L. Tang, A. Qin, R. Hu, J. Z. Sun and B. Z. Tang, *J. Am. Chem. Soc.*, 2011, **133**, 660–663; (c) H. Shi, J. Liu, J. Geng, B. Z. Tang and B. Liu, *J. Am. Chem. Soc.*, 2012, **134**, 9569–9572; (d) S. Chen, Y. Hong, Y. Liu, J. Liu, C. W. T. Leung, M. Li, R. T. K. Kwok, E. Zhao, J. W. Y. Lam, Y. Yu and B. Z. Tang, *J. Am. Chem. Soc.*, 2013, **135**, 4926–4929; (e) Y. Yuan, R. T. K. Kwok, B. Z. Tang and B. Liu, *J. Am. Chem. Soc.*, 2014, **136**, 2546–2554.

19   R. Hu, E. Lager, A. Aguilar-Aguilar, J. Liu, J.W. Y. Lam, H. H. Y. Sung, I. D. Williams, Y. Zhong, K. Si. Wong, E. Peña-Cabrera and B. Z. Tang, *J. Phys. Chem. C*, 2009, **113**, 15845–15853.

20   X. Y. Shen, W. Z. Yuan, Y. Liu, Q. Zhao, P. Lu, Y. Ma, I. D. Williams, A Qin, J. Zhi Sun and B. Z. Tang, *J. Phys. Chem. C*, 2012, **116**, 10541–10547.

21   X. Y. Shen, Y. J. Wang, E. Zhao, W. Z. Yuan, Y. Liu, P. Lu, A. Qin, Y. Ma, J. Z. Sun and B. Z. Tang, *J. Phys. Chem. C*, 2013, **117**, 7334–7347.

22   B.-R. Gao, H.-Y. Wang, Y.-W. Hao, L.-M. Fu, L.-H. Fang, Y. Jiang, L. Wang, Q.-D. Chen, H. Xia, L.-Y. Pan, Y.-G. Ma and H.-B. Sun, *J. Phys. Chem. B*, 2010, **114**, 128–134.

23   B.-R. Gao, H.-Y. Wang, Z.-Y. Yang, H. Wang, L. Wang, Y. Jiang, Y.-W. Hao, Q.-D. Chen, Y.-P. Li, Y.-G. Ma and H.-B. Sun, *J. Phys. Chem. C*, 2011, **115**, 16150–16154.

24   T. Ishi-i, K. Ikeda, Y. Kichise and M. Ogawa, *Chem. Asian J.*, 2012, **7**, 1553–1557.

25   T. Ishi-i, R. Hashimoto and M. Ogawa, *Asian. J. Org. Chem.*, 2014, **3**, 1074–1082.

26   S. Kato, T. Matsumoto, M. Shigeiwa, H. Gorohmaru, S. Maeda, T. Ishi-i and S. Mataka, *Chem. Eur. J.*, 2006, **12**, 2303–2317.

27   J. Massin, A. Charaf-Eddin, F. Appaix, Y. Bretonnière, D. Jacquemin, B. van der Sanden, C. Monnereau and C. Andraud, *Chem. Sci.*, 2013, **4**, 2833–2843.

28   C. Reichardt, *Chem. Rev.*, 1994, **94**, 2319-2358.

29   (a) A. Marini, A. Muñoz-Losa, A. Biancardi and B. Mennucci, *J. Phys. Chem. B*, 2010, **114**, 17128–17135; (b) J. Do, J. Huh and E. Kim, *Langmuir*, 2009, **25**, 9405–9412; (c) C. Bohne, H. Ihmels, M. Waidelich and C. Yihwa, *J. Am. Chem. Soc.*, 2005, **127**, 17158–17159; (d) F. D. Lewis and J.-S. Yang, *J. Am. Chem. Soc.*, 1997, **119**, 3834–3835; (e) A. Suzuki, N. Nemoto, I. Saitob and Y. Saito, *Org. Biomol. Chem.*, 2014, **12**, 660–666.

30   P. Strohriegl and J. V. Gazulevicius, *Adv. Mater.*, **2002**, 14, 1439–1452.

31   D. Gcrl, X. Zhang and F. Würthner, *Angew. Chem. Int. Ed.*, 2012, **51**, 6328–6348.

32   (a) S. Kato, T. Matsumoto, M. Shigeiwa, H. Gorohmaru, S. Maeda, T. Ishi-i and S. Mataka, *Chem. Commun.*, 2004, 2342–2343; (b) T. Ishi-i, N. Nakamura, T. Mine, S. Imamura, M. Shigeiwa, H. Gorohmaru and S. Maeda, *Chem. Lett.*, 2009, **38**, 1042–1043.

33   T. Ishi-i, M. Sakai and C. Shinoda, *Tetrahedron*, 2013, **69**, 9475–9480.

34   J. V. Caspar, E. M. Kober, B. P. Sullivan and T. J. Meyer, *J. Am. Chem. Soc.*, 1982, **104**, 630–632.

35   (a) C. Gota, S. Uchiyama, T. Yoshihara, S. Tobita and T. Ohwada, *J. Phys. Chem. B*, 2008, **112**, 2829–2836; (b) S. Uchiyama, K. Kimura, C. Gota, K. Okabe, K. Kawamoto, N. Inada, T. Yoshihara and S. Tobita, *Chem. Eur. J.*, 2012, **18**, 9552–9563.

36   A. L. Macanita, F. P. Costa, S. M. B. Costa, E. C. Melo and H. Santos, *J. Phys. Chem.*, 1989, **93**, 336–343.

37   K. Kudo, A. Momotake, Y. Kanna, Y. Nishimura and T. Arai, *Chem. Commun.*, 2011, **47**, 3867–3869.

38   M. J. Kamlet, J. L. M. Abboud, M. H. Abraham and R. W. Taft, *J. Org. Chem.*, 1983, **48**, 2877–2887.

39   (a) Y. Ren, Y. Q. Dong, J. W. Y. Lam, B. Z. Tang and K. S. Wong, *Chem. Phys. Lett.*, 2005, **402**, 468–473; (b) Y. Ren, W. Y. Lam, Y.

Organic & Biomolecular Chemistry Accepted Manuscript

Q. Dong, B. Z. Tang and K. S. Wong, *J. Phys. Chem. B*, 2005, **109**, 1135–1140.

40 B. Valeur and M. N. Berberan-Santos, *Molecular Fluorescence: Principles and Applications*, Wiley-VCH, Weinheim, 2nd revised ed., 2012, Chapter 10.1..

41 M. Kasha, H. R. Rawls and M. A. El-Bayoumi, *Pure Appl. Chem.*, 1965, **11**, 371–392.

42 A small-angle X-ray scattering measurement showed a formation of micellar-type aggregate with a diameter of ca. 5.7 nm (Fig. S24†). The size of the micellar-type aggregate coincides with a model predicted from the molecular size (extended molecular size of ca. 4 nm and aromatic core size of ca. 1.7 nm). Detailed results will be reported elsewhere.

43 (a) S. R. Marder, *Chem. Commun.*, 2006, 131–134; (b) G. S. He, L.-S. Tan, Q. Zheng and P. N. Prasad, *Chem. Rev.*, 2008, **108**, 1245-1330; (c) S. Sumalekshmy and C. J. Fahrni, *Chem. Mater.*, 2010, **23**, 483–500.

44 M. T. Stone and J. S. Moore, *Org. Lett.*, 2004, **6**, 469–472.

45 K. Suzuki, A. Kobayashi, S. Kaneko, K. Takehira, T. Yoshihara H. Ishida, Y. Shiina, S. Oishi and S. Tobita, *Phys. Chem. Chem. Phys.*, 2009, **11**, 9850–9860.